Supporting Information for "Sources and pathways of polycyclic aromatic hydrocarbons transported to Alert, the Canadian High Arctic"

RONG WANG,[+] SHU TAO,[+*] BIN WANG,[+] YU YANG,[+] CHANG LANG,[+] YANXU ZHANG,[+] JING HU[+], JIANMIN MA,[‡] HAYLEY HUNG[‡]

Laboratory for Earth Surface Processes, College of Urban and Environmental Sciences, Peking University, Beijing 100871, China. [‡]Air Quality Research Division, Science and Technology Branch, Environment Canada, 4905 Dufferin Street, Toronto, Ontario M3H 5T4, Canada

[+] Peking University

[‡] Science and Technology Branch, Environment Canada

[*] Corresponding author phone and fax: 0086-10-62751938; email: taos@urban.pku.edu.cn

This material includes 14 pages, 8 figures, and 6 tables.

S1 Updated Global PAH Emission Inventory

The global emission inventory developed previously by Zhang et al. (*1*) was used in this study. The inventory was further updated by replacing the emission factors of aluminum electrolysis and petroleum fuel for high-income countries with the lately published data (*2, 3*). The updated global emission inventory for the total of the 15 PAHs studied is mapped in Figure S1.

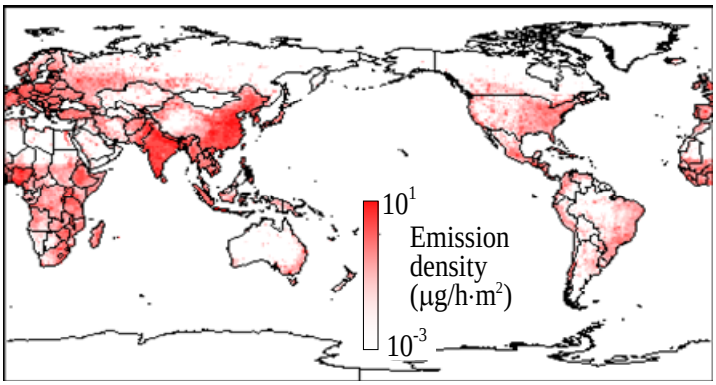

Figure S1. The updated global emission density for the total of the 15 PAHs studied.

S2 Modeling

As presented in Figure S2, 10 backward air mass trajectories starting from various heights from 100 to 1000 m above the ground at Alert were calculated. For a trajectory entering a given grid (x, y) at trajectory time i with a period of j hours staying in the grid, the local contributions to the receptor at Alert during the j hours from the hour i to hour i+j were integrated.

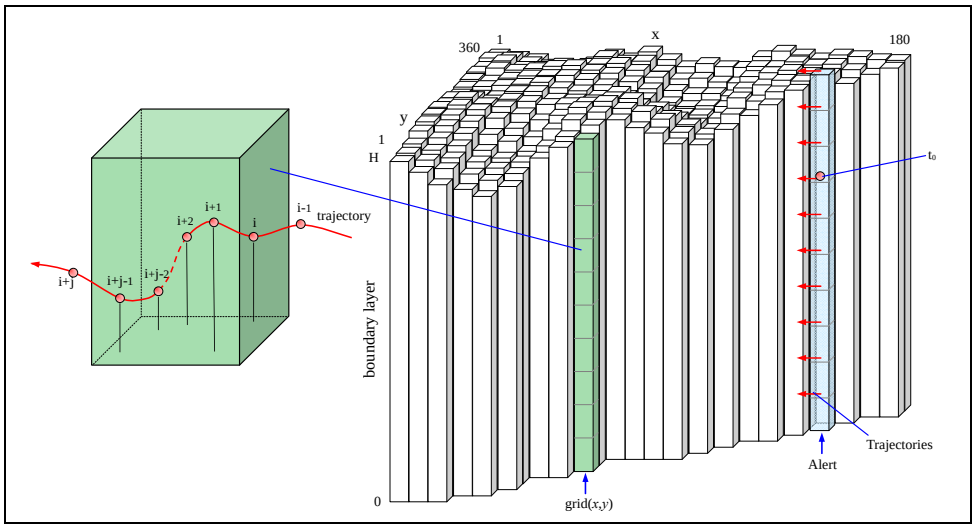

Figure S2. Graphical presentation of the $ISCF_{hxy}$ calculation showing the 10 starting points of trajectories at Alert (blue column, t = 0), grids with various atmospheric boundary layer heights, and the time steps of a trajectory passing a given grid (green column, x, y) (t=i, i+1, …, i+j). A section of the grid is shown on the left with time steps of a trajectory passing through it.

S3 Derivation of Model Parameters.

Dry deposition velocity (v_d) was calculated using a method provided by MSCE-POPs model (*4*). The daily atmospheric boundary layer heights (H) were from Can METOP model (1°×1°), calculated based on the sub-grid scale surface heterogeneity and meteorological condition (*5*). Atmospheric OH radical concentration ($[OH]$) and volume fraction of atmospheric particles (X) were from Harvard University GEOS-CHEM monthly archived global data set (2°×2.5°) (*6*). Precipitation rate (I) and atmospheric ambient temperature (T) were derived from global NOAA-NCEP/NCAR pressure level reanalysis data archive (*7*).

According to the partitioning equation between gaseous and particulate phases by Mackay et al (*8*), the fraction of particle-phase PAHs (f_p) is calculated in **eq S1** as a function of T (K) and X (v/v) en-route.

$$f_p = \frac{1}{1 + \frac{A \cdot e^{B\left(\frac{1}{298} + \frac{1}{T}\right)}}{6 \times 10^6 X}}, \qquad \text{(S1)}$$

A and B are regression coefficients derived based on the measured gaseous and particulate phase PAHs concentrations together with the measured temperature at Alert in 2000, which were also provided by

Northern Contaminants Program. The calculated *A* and *B* values are presented in Table S1.

Table S1 Results of the regression modeling for the partition between gaseous and particulate phase PAHs

PAHs	*A*	*B*	r^2	*P value in regression*
ACY	1.04×10^{-5}	-2.77×10^{3}	0.38	0.01
ACE	8.38×10^{-6}	-4.29×10^{3}	0.55	0.01
FlO	8.99×10^{-5}	-4.18×10^{3}	0.48	0.01
PHE	2.78×10^{-3}	5.93×10^{3}	0.50	0.01
ANT	4.99×10^{-4}	4.19×10^{3}	0.35	0.01
FLA	1.44×10^{-3}	7.67×10^{3}	0.46	0.01
PYR	1.13×10^{-3}	7.62×10^{3}	0.55	0.01
BaA	5.27×10^{-5}	5.97×10^{3}	0.56	0.01
CHR	1.15×10^{-4}	7.68×10^{3}	0.61	0.01
BbF	1.00×10^{-4}	8.59×10^{3}	0.59	0.01
BkF	5.81×10^{-5}	6.55×10^{3}	0.55	0.01
BaP	2.70×10^{-5}	4.39×10^{3}	0.45	0.01
IcdP	7.07×10^{-5}	7.67×10^{3}	0.59	0.01
DahA	2.05×10^{-5}	2.82×10^{3}	0.32	0.05
BghiP	5.11×10^{-5}	6.40×10^{3}	0.50	0.01

The total wet deposition scavenging ratio (S_c) was calculated based on f_p using **eq S2,3** by regression models for rain and snow from Franz et al. (*9*), respectively:

$$\log S_c = 0.37\log f_p + 4.0 \qquad \left(r^2 = 0.76\right), \qquad rain, \tag{S2}$$

$$\log S_c = 0.89\log f_p + 6.1 \qquad \left(r^2 = 0.53\right), \qquad snow. \tag{S3}$$

Reaction rate constants for PAHs listed in Table S2 were after Yan et al. who derived these values using a LFERs (polyparameter linear free energy relationships) model (*10*).

Table S2 Reaction rate constants for the reaction between PAHs and OH radicals

PAHs	K_{OH}, cm^3/molecules·s
ACY	$1.10\pm0.00\times10^{-10}$
ACE	$5.56\pm0.34\times10^{-11}$
FlO	$1.46\pm0.22\times10^{-11}$
PHE	$1.74\pm0.62\times10^{-11}$
ANT	$1.43\pm0.46\times10^{-10}$
FLA	$3.69\pm1.85\times10^{-11}$
PYR	$8.20\pm4.53\times10^{-11}$
BaA	$7.60\pm3.68\times10^{-11}$
CHR	$6.57\pm2.02\times10^{-11}$
BbF	$1.91\pm0.06\times10^{-11}$
BkF	$5.23\pm0.18\times10^{-11}$
BaP	$1.56\pm1.50\times10^{-10}$
IcdP	$8.00\pm2.19\times10^{-11}$
DahA	$6.33\pm1.88\times10^{-11}$
BghiP	$4.98\pm5.25\times10^{-11}$

All the parameters are summarized as follows:

x,y	the meridian and zonal grid coordinates
s	time step of the trajectory calculation
t	trajectory time
τ	transport time from a given grid to the receptor (Alert in this study)
T	atmospheric ambient temperature
I	precipitation rate
H	atmospheric boundary layer height
X	volume fraction of atmospheric particles
$[OH]$	atmospheric OH radical concentration
M	remaining fraction of pollutant after transported from a given grid to the receptor
L	pollutant loading at a given grid
V_b	weighting factor for the pollutant loading at different heights in source grids

E	emission flux at a given grid
K_τ	decay constant during a period from τ to τ+1
f_P	fraction of particulate phase PAHs
v_d	dry deposition velocity
S_c	total wet deposition scavenging coefficient
K_{OH}	reaction rate constant of PAHs with OH radicals.

S4 Seasonal Variation in Descending Motion at Alert

To describe the seasonal variation in air mass descending motion at Alert, the vertical directions (either up or down) of air mass movement 100 m above the ground from HYSPLIT trajectory calculation at Alert were recorded every 6 hours for each month based on the meteorology data in the global NOAA-NCEP/NCAR pressure level reanalysis data archive (7). The percentage of the descending motion was derived and presented in Figure S3. It appears that the descending motion of air mass at Alert was weaker in March, July and October than that in the other months.

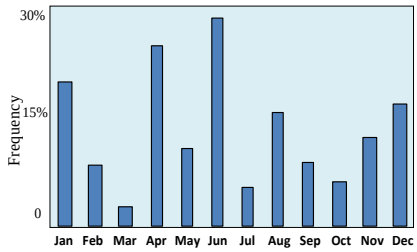

Figure S3. Monthly variation in frequency of air mass descending motion at 100 m above the ground at Alert.

S5 Validation for Model Predicted $ISCF(N)_n$ for the other PAHs

In the main text, the time series of the model predicted $ISCF(N)_n$ values were compared with the concentrations observed at Alert in 2004 for FLA and PYR, which were the only two compounds with all the measured concentration above the detection limits. Figure S4 shows the results of another 11 PAHs with the measured winter concentrations above the detection limits and summer concentrations below the detection limits. Of the 15 PAHs, all measured concentrations of ACE and ANT over the studied period were below their detection limits and hence they were not compared with the model predictions. As shown in the figure, there are discrepancies between modeled and measured results. These are likely due to the uncertainty in the parameters of the model and local reemissions, as well as measurement errors, especially for these under detection limits. The vertical movement can also cause the discrepancy as predicted *ISCF*

for the layer 100-1000 meters high would impact on the ground concentration weakly when the ascending movement is frequent.

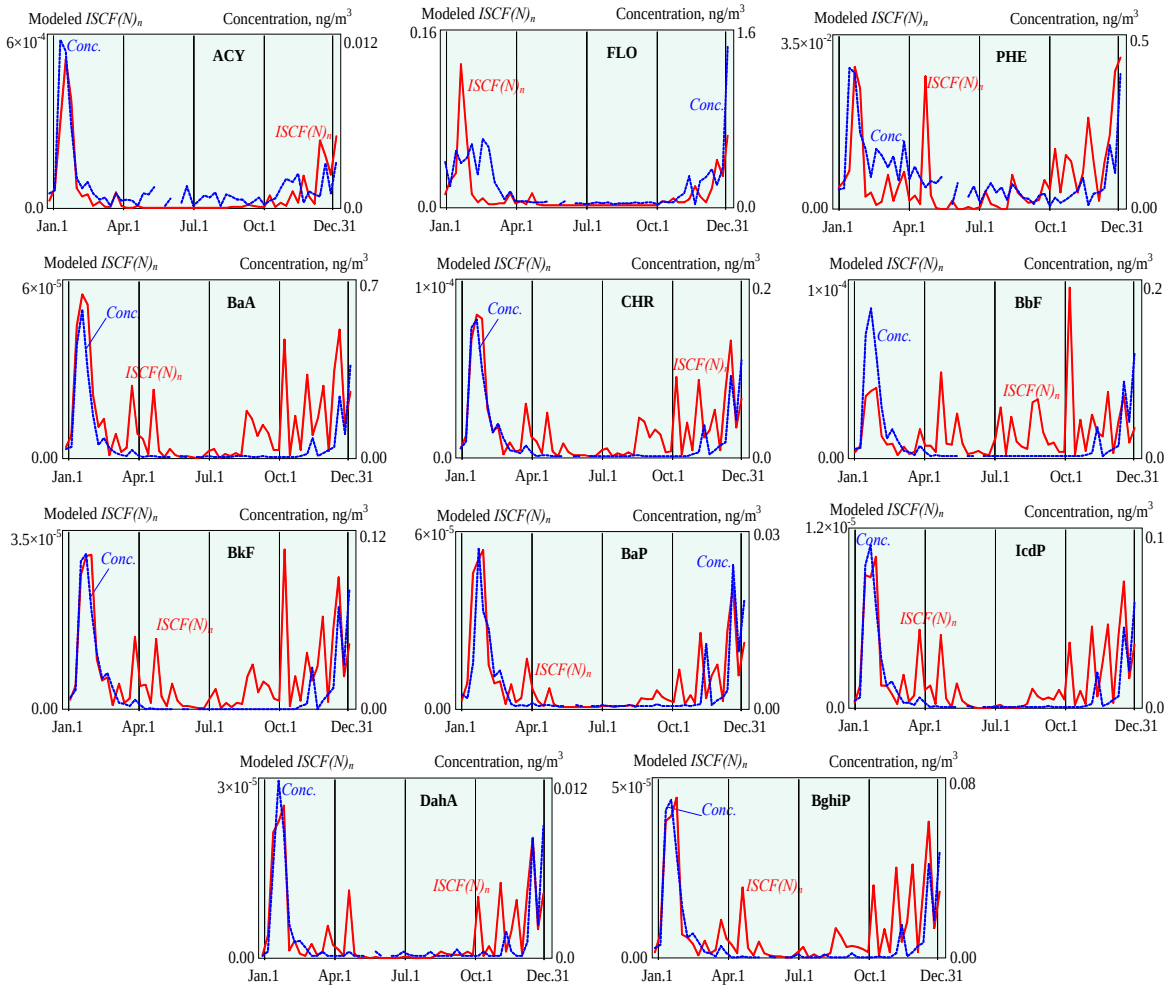

Figure S4. Comparison in the time series of individual PAHs between the model predicted $ISCF(N)_n$ as the average for layer 100-1000 m above ground and the field observed concentrations at ground in 2004 for the 11 PAHs with the measured winter concentrations above the detection limits and summer concentrations below the detection limits.

S6 Geographical Distributions of Source Contributions for FLO, PYR and BaP

The annual mean *ISCF(N)* values for FLO, PYR, and BaP in 2004 are mapped in Figure S5, showing the major source regions for Alert. The majority of PAHs occurred at Alert were from the Northern Hemisphere through long-range transport. The three major source regions were North Europe (including European Russian), North America (Canada and the eastern United States), and East Asia.

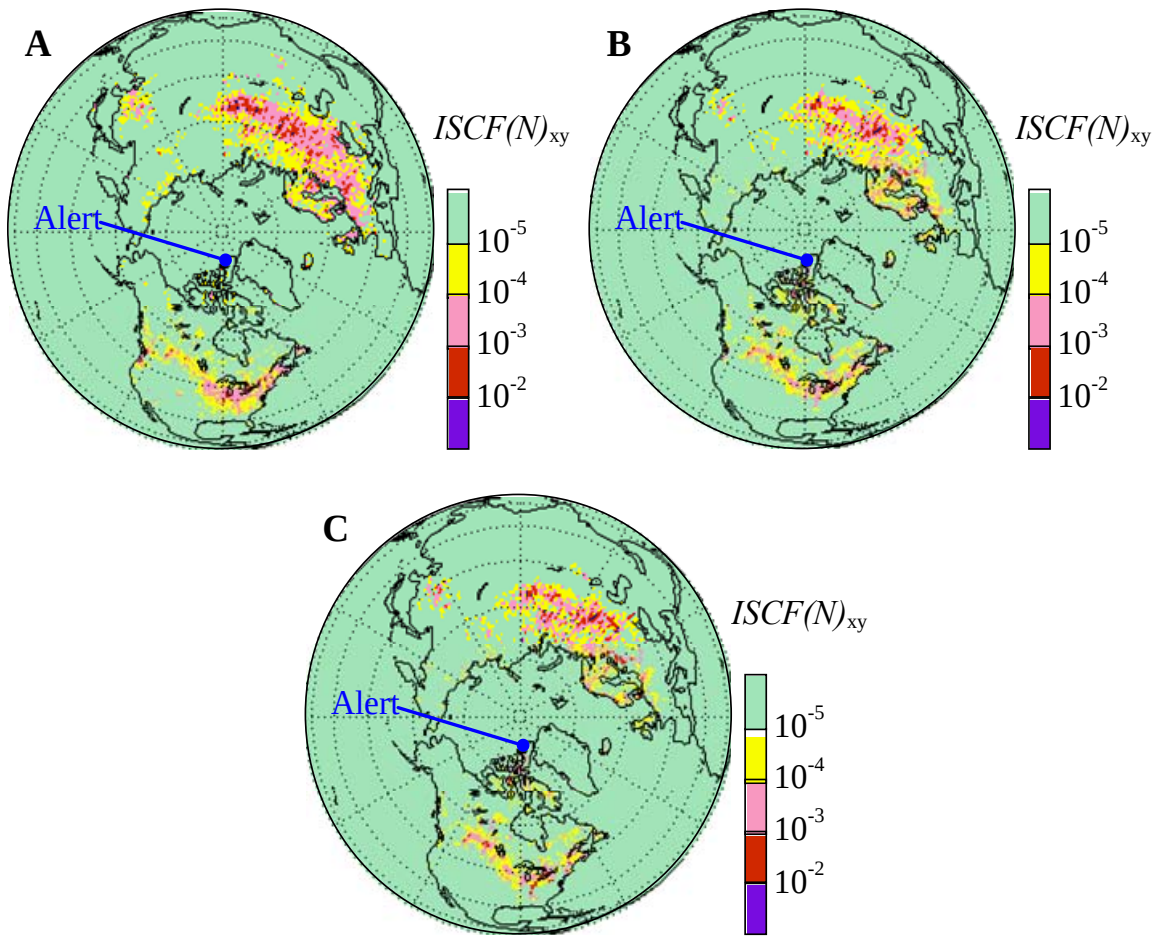

Figure S5. Geographical distributions of annual mean $ISCF(N)_{xy}$ values of FLO (A), PYR (B), and BaP (C) representing the global distributions of source regions of PAHs observed at Alert.

Based on the calculated $ISCF(N)_{xy}$, the relative contributions of major emission activities were derived and listed in Table S3 for PAH15 and the three representative PAHs (FLO, PYR, and BaP)

Table S3 Relative contributions of various emission activities to PAHs observed at Alert.

PAHs	domestic coal, %	biofuel burning, %	aluminum electrolysis, %	petroleum fuel, %	waste incineration, %	coke production, %	all other sources, %
PAH15	23	24	23	7	7	5	26
FLO	24	24	22	11	6	8	6
PYR	7	16	27	9	11	5	24
BaP	14	18	33	6	14	11	5

S7 Seasonal Variations in Spatial Distributions of Source Contributions for FLO, PYR and BaP

In addition to the seasonality of geographical distribution of source contributions for PAH15, results for individual PAH compounds were derived. In Figures S6-S8, the results of the three representative PAHs, FLO, PYR and BaP are presented, respectively. In general, the spatial distribution patterns were similar to one another. Difference existed mainly in the relative contributions of various regions. For example, China emission contributed more for FLO (19%) in spring than PYR (6%) as the OH reaction rate constant for PYR was five times higher than that for FLO, while PAHs from China traveled longer distance than those from the other source regions.

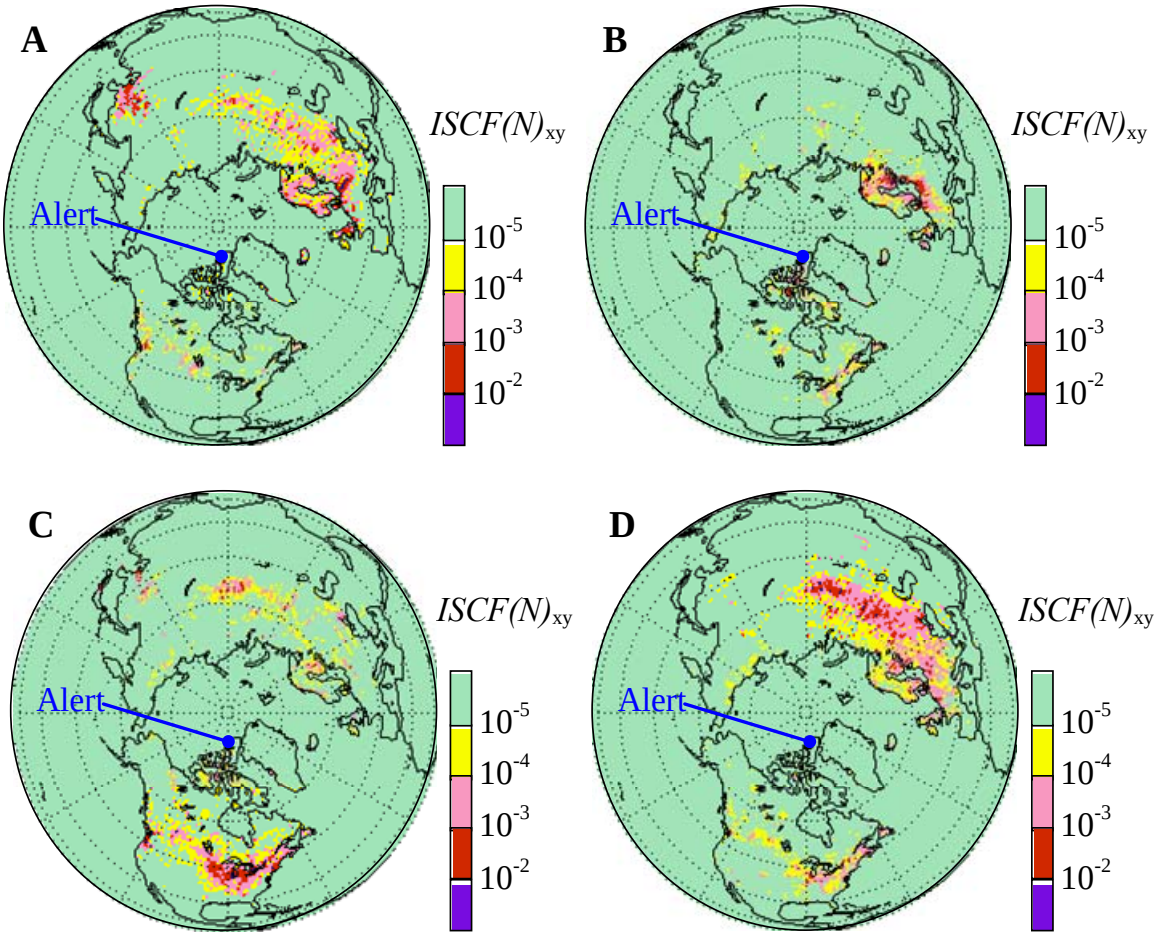

Figure S6. Geographical distributions of seasonal mean $ISCF(N)_{xy}$ values of FLO representing the global distributions of source regions of FLO observed at Alert in the four seasons. **A**. Spring, **B**. Summer, **C**. Fall, **D**. Winter.

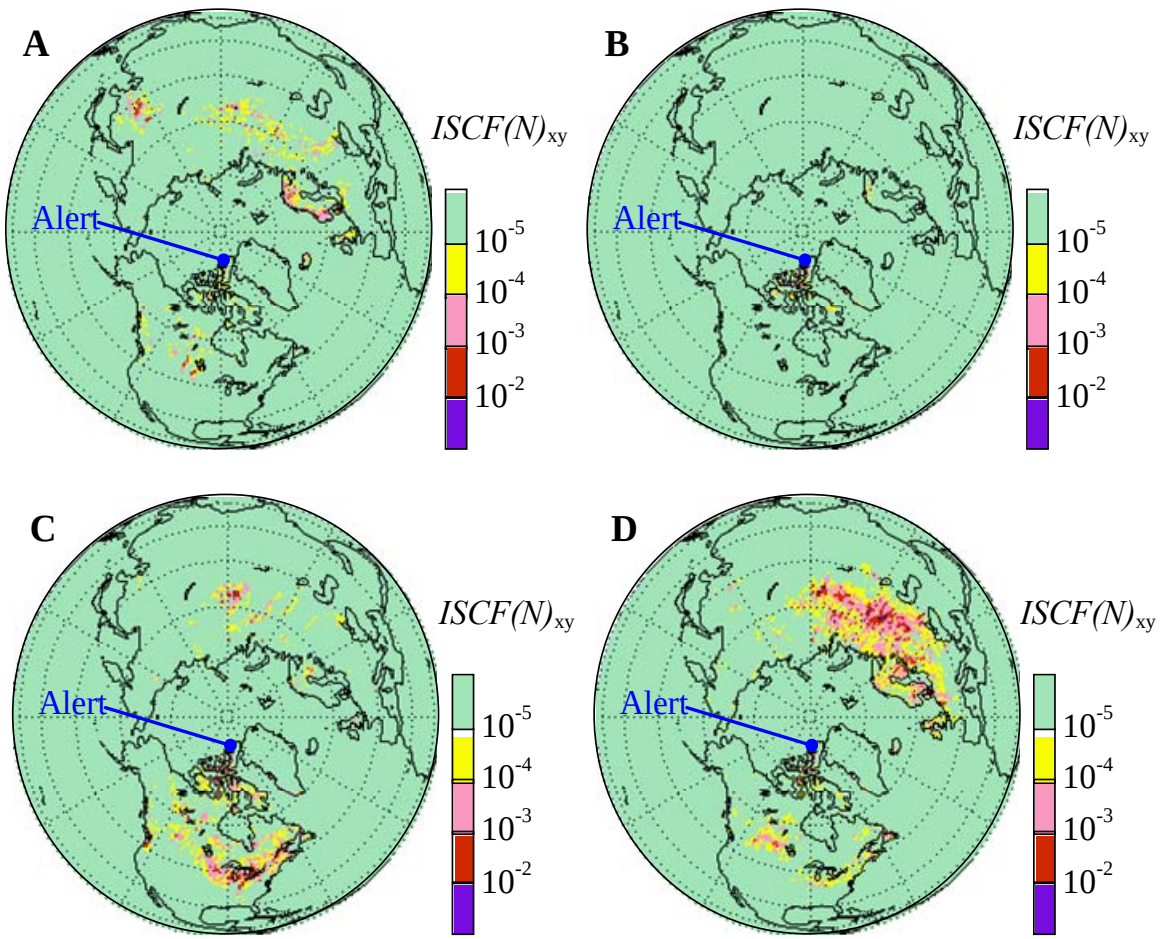

Figure S7. Geographical distributions of seasonal mean $ISCF(N)_{xy}$ values of PYR representing the global distributions of source regions of PYR observed at Alert in the four seasons. **A**. Spring, **B**. Summer, **C**. Fall, **D**. Winter.

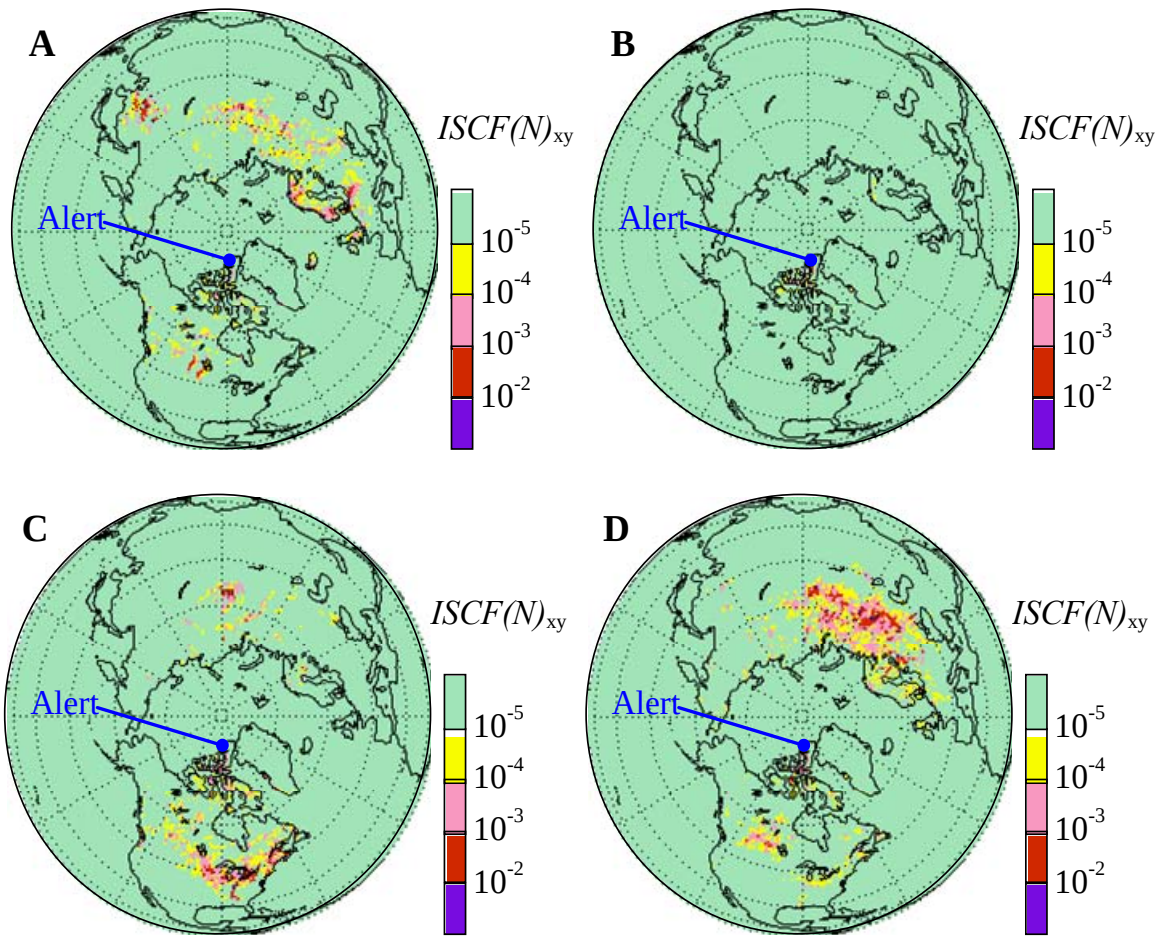

Figure S8. Geographical distributions of seasonal mean $ISCF(N)_{xy}$ values of BaP representing the global distributions of source regions of BaP observed at Alert in the four seasons. **A**. Spring, **B**. Summer, **C**. Fall, **D**. Winter.

S8 Seasonal Variation in Source Contributions to FLO, PYR, and BaP at Alert

Table S4 lists the contributions of major geographical regions to the atmospheric level of PAHs at Alert. The results highlight the difference among the regions and the difference among the individual PAH compounds. For example, only 7.1% of FLO was from Canada but the percentage of BaP from Canada reached 20%.

Table S4 Relative contributions of various source regions to the PAHs at Alert.

PAHs	East Asia %	European Russia, %	North/West Europe, %	Canada %	USA %	Greenland %
PAH15	25	34	11	17	8.0	5.7

FLO	29	41	14	7.1	7.6	0.3
PYR	20	30	9.3	16	2.1	21
BaP	23	40	7.3	20	4.9	4.8

The information on contributions of all emission activities and source regions was also broken down to the four seasons to show the seasonality of the sector and regional contributions to PAHs at Alert (Tables S5 and S6). Differences in seasonal patterns of the relative contributions among the major emission activities and the source regions are well demonstrated.

Table S5 Seasonal variation in the relative contribution of various activities to PAH15 at Alert

season	domestic coal, %	biofuel burning, %	aluminum electrolysis, %	petroleum fuel, %	waste incineration, %	coke production, %	all other sources, %
spring	13	31	21	7.3	4.0	5.3	17
summer	3.3	40	21	9.0	0.4	3.3	23
fall	10	30	17	12	5.5	3.9	20
winter	27	18	25	4.1	6.6	5.5	15
annual	23	24	23	6.4	6.6	5.4	26

Table S6 Seasonal variation in the relative contribution of various source regions to PAH15 at Alert.

season	East Asia %	European Russia, %	North/West Europe, %	Canada %	USA %	Greenland %
spring	26	5.1	46	6.4	0.4	16
summer	0.4	1.4	5.1	76	0.1	17
fall	16	1.7	0.7	38	32	12
winter	24	55	9.8	9.7	1.1	0.6
annual	25	34	11	17	8.0	5.7

Literature Cited

[1] Zhang, Y. X.; Tao, S. Global atmospheric emission inventory of polycyclic aromatic hydrocarbons (PAHs) for 2004. *Atmos. Environ.* **2009**, *43*, 812-819.

[2] Environment Canada. 2000 criteria air contaminant Emission Inventory; Pollution Data Division: Ottawa, 2004.

[3] Ketzel, M.; Wahlin, P.; Berkowicz, R.; Palmgren, F. Particle and trace gas emission factors under urban driving conditions in Copenhagen based on street and roof-level observations. *Atmos. Environ.* **2003**, *37*, 2735-2749.

[4] Pistocchi, A. A GIS-based approach for modeling the fate and transport of pollutants in Europe. *Environ. Sci. Technol.* **2008**, *42*, 3640-3647.

[5] Zhang, L. S.; Ma, J. M.; Venkatesh, S.; Li, Y. F.; Cheung, P. Modeling Evidence of Episodic Intercontinental Long-Range Transport of Lindane. *Environ. Sci. Technol.* **2008**, *42*, 8791-8797.

[6] Harvard University GEOS-Chem program: GEOS-CHEM monthly archived global data (2×2.5 degree resolution). Available at http://www-as.harvard.edu/chemistry/trop/geos/geos_hi_res.html.

[7] NOAA Air Resources Laboratory: Global NOAA-NCEP/NCAR pressure level reanalysis data archive. Available at http://www.gus.arlhq.noaa.gov/pub/archives/reanalysis.

[8] Mackay, D. *Multimedia Environmental Models: the fugacity approach*; Lewis Publishers: Boca Raton, FL, 2000.

[9] Franz, T. P.; Eisenreich, S. J. Snow scavenging of polychlorinated biphenyls and polycyclic aromatic hydrocarbons in Minnesota. *Environ. Sci. Technol.* **1998**, *32*, 1771-1778.

[10] Yan, C. L.; Chen, J. W.; Huang, L. P.; Ding, G. H.; Huang, X. Y. Linear free energy relationships on rate constants for the gas-phase reactions of hydroxyl radicals with PAHs and PCDD/Fs. *Chemosphere* **2005**, *61*, 1523-1528.